Phonon and plasmon deformation potentials of GaAs: Far-infrared study under uniaxial stress

M. Hünermann, W. Richter, and J. Saalmüller
I. Physikalisches Institut, Rheinisch-Westfälische Technische Hochschule Aachen, D-5100 Aachen, Federal Republic of Germany

E. Anastassakis
Physics Laboratory III, National Technical University, Zografau Campus, Athens, 15773, Greece
(Received 2 December 1985; revised manuscript received 30 June 1986)

We report the results of a complete study of the effects of a uniaxial stress on the far-infrared reflectivity spectrum of GaAs. Stresses up to 15 kbar applied along the [111] and [001] directions allowed us to measure splittings of phonon degeneracies and frequency shifts of the long-wavelength TO and LO phonons and of the free-carrier plasma frequency. From these results we were able to calculate the phonon and plasmon deformation potentials. More importantly, numerical values are obtained for the rate of shifts of the electron effective mass. The results are compared with values given in the literature.

I. INTRODUCTION

When a uniaxial stress is applied to a crystal, definite changes occur in the lattice-dynamical, electronic, and optical behavior of the material. Shifts of the long-wavelength ($q \approx 0$) optical phonons and splittings of their degeneracies are manifestations of such stress-induced lattice-dynamical changes, from which useful crystal parameters can be obtained. Diamond-type cubic materials, fluorites and III-V semiconductors are among the structures most extensively studied.[1] Most of these studies are based on piezo-Raman spectroscopic measurements. The alternative approach of using effects of stress on the reflectivity spectra has received limited attention thus far, and in fact has been applied only once, in the case of GaAs,[2] in spite of the fact that such data appear to be more informative. Thus the complete set of phonon deformation potentials (PDP), i.e., the rates of shifts of transverse (TO) and longitudinal (LO) optical phonons with the strains can be obtained with improved accuracy, since the incident radiation penetrates deeper into the material thus probing areas with more uniform strains. On the contrary, piezo-Raman experiments are subject to more stringent selection rules and are more sensitive to strain inhomogeneities because of the shorter penetration depths reached by incident laser light.[3,4] The main advantage of the reflectance measurements under uniaxial stress, however, is the possibility to study the stress effects on free carrier parameters, such as effective masses, through the changes of plasma frequency with the strains (plasmon deformation potentials or PLDP). In principle, one can also obtain information about the phonon damping deformation potentials (PDDP), and about the high- and low-frequency photoelastic constants. Such results, however, require very accurate spectra and elaborate fitting techniques.

The purpose of this work is to use reflectance data from uniaxial stress measurements in GaAs obtained under improved experimental conditions to reach accurate values for PDP and PLDP. Such PDP values have been extensively used in recent years in determining quantitatively, residual tensile or compressive strains on bulk or epitaxial films of Si or III-V semiconductors,[5,6] in connection with epitaxial film growing, surface treatment, laser annealing, and ion implantation processes. Furthermore, PDP can be used to obtain the dispersion of the photoelastic and elasto-optical coefficients in the infrared, and also to estimate the changes induced on the phonon effective charge by external stresses or hydrostatic pressures.[7] Not much information is available about electronic properties in strained lattices. Such data, e.g., effective mass m^*, carrier mobility μ or scattering time τ, as a function of strain are of crucial importance for the evaluation of the transport properties of epitaxial layers used in the fabrication of microelectronic components.[5,6] Values for such strain parameters have been suggested by theoretical calculations.[8]

In Sec. II the experimental details will be described, followed in Sec. III by the basic theoretical facts and data, leading to the listing of PDP values and values for crystal parameters based on them. A short discussion on the effect of strains on the phonon damping constant is given in Sec. IV, while in Sec. V the results on the PLDP are presented together with relevant theoretical facts, followed by a discussion and closing remarks.

II. EXPERIMENTAL

Reflectivity spectra in the range from 80 to 370 cm^{-1} were taken with a rapid scan Fourier spectrometer. The total path difference scanned was 4.15 cm yielding a spectral resolution of 0.13 cm^{-1}. The interferograms contained 4096 data points. In order to separate the singlet and doublet phonon components the light was polarized to more than 92% by a wire grid polarizer.

Pure and doped GaAs samples were cut in the form of rectangular bars of typical dimensions $2\times2\times15$ mm^3. The reflecting surfaces were polished (1 μm diamond) and etched carefully (1% Br_2 in methanol, 5 min). The etching turned out to be very important in order to obtain the

high accuracy in fitting the reflectivity spectra and establishing the frequency shifts with stress. Unetched samples showed differences in the reflectivity of up to 10%, especially in the region of the plateau of the reststrahlen band. Two sample orientations were used designated by $(x',y',z')=([110],[\bar{1}10],[001])$ or b and $(x'',y'',z'')=([\bar{1}10],[\bar{1}\bar{1}2],[111])$ or c (see Fig. 1 and Ref. 4). The long axis of the bars was z' or z''. The stress was always applied along the long axis. Incidence of light was along x',x''. The stress apparatus was newly designed[9] in order to overcome the geometrical problems experienced with the conventional Γ-shaped design.[10] Maximal forces up to 5000 N could be applied to the sample. The samples, with their end faces polished, were held by friction (no glue) between two steel pistons, whose faces were also polished and covered by small pieces of fused silica. With such an arrangement we were able to exceed the limits of previously applied stresses before breaking the sample (14.2 kbar for $\mathbf{X}||[111]$ and 7.5 kbar for $\mathbf{X}||[001]$). In addition, accidental breaking for low stresses was minimized.

In usual reflectivity measurements absolute values for the reflectivity R are established by using a metallic mirror as a reflectivity standard and exchanging sample and mirror in a well-defined manner. The latter, however, is hardly possible with a sample held in a bulky and heavy stress apparatus. Therefore, the following experimental procedure was followed: First the sample without stress apparatus was measured very carefully against a metallic standard mirror. From this measurement the reflectivity, $R(\omega, X=0)$, was determined as a function of frequency at zero stress, X,

$$R(\omega, X=0)=\frac{I(\omega, X=0)}{I_{\text{mirror}}(\omega)} , \tag{1}$$

where I, I_{mirror} are the corresponding reflected intensities. Then the sample was mounted in the stress apparatus and the intensity of reflected light $I'(\omega,X)$ was measured for $X=0$ and $X\neq 0$. From such measurements the following ratio is established:

$$\frac{I'(\omega,X)}{I'(\omega, X=0)}=\frac{R(\omega,X)}{R(\omega, X=0)} , \tag{2}$$

from which

$$R(\omega,X)=\frac{I'(\omega,X)}{I'(\omega, X=0)} R(\omega, X=0) . \tag{3}$$

Typical spectra for $R(\omega, X=0)$, $R(\omega,X)$, and the ratio $R(\omega,X)/R(\omega, X=0)$ are displayed in Figs. 2(a) and 2(b).

III. PHONON DEFORMATION POTENTIALS

A. General information and experimental procedure

The phenomenological treatment of the effects of an uniaxial stress on the $q\approx 0$ TO- and LO-phonon frequencies is well established and details can be found in Refs. 1–3. Shifts of the frequencies and splittings of their degeneracies can be expressed in terms of the phonon deformation fourth-rank tensor $(\partial\Omega^2/\partial\eta)_{ij}$, in suppressed index notation. By Ω and η we designate the perturbed angular frequency of the phonon and the strain. For diamond-type and zinc-blende–type crystals the above tensor has three independent components, designated by p, q, and r or K_{11}^{Γ}, K_{12}^{Γ}, and K_{44}^{Γ} for a TO phonon, and by

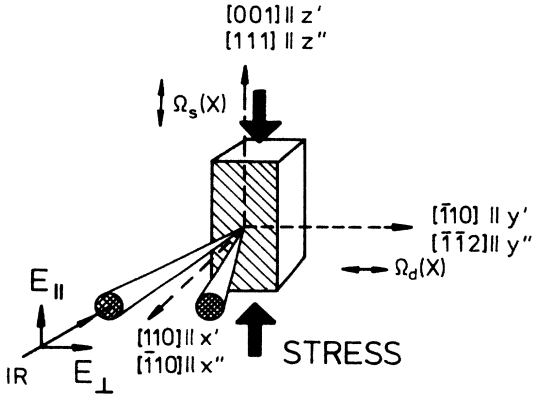

FIG. 1. Experimental configurations used in the present measurements. The sample configurations (b,c) used are b: $(x',y',z')=([110],[\bar{1}10],[001])$ and c: $(x'',y'',z'')=([\bar{1}10],[\bar{1}\bar{1}2],[111])$. Double arrows indicate the singlet and doublet modes of vibration.

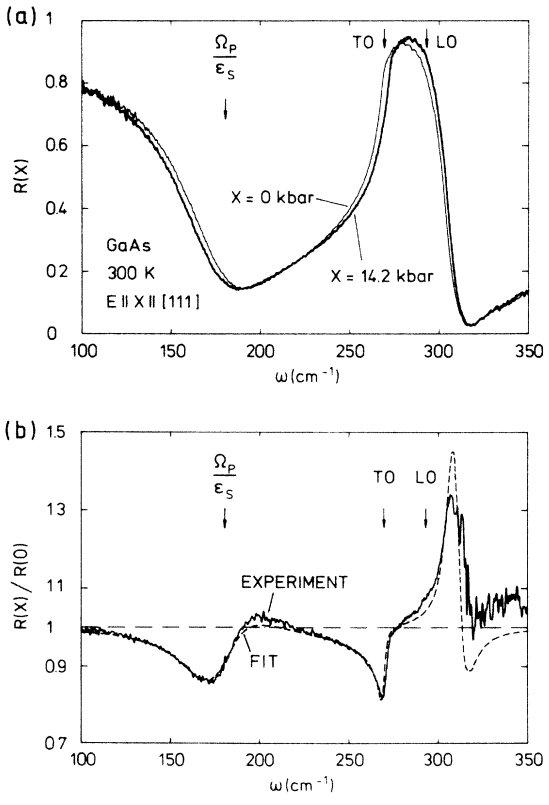

FIG. 2. (a) Reflectivity spectra with $X=0$ and $X=14.2$ kbar along [111]. The sample is doped with $N=3.5\times10^{17}$ cm^{-3}. The position of the phonon frequencies and the reflectivity edge at Ω_P/ϵ_s are indicated by arrows. (b) Experimental and theoretical spectrum of the ratio $R(X)/R(0)$ based on (a).

p', q', and r' or K_{11}^{L}, K_{12}^{L}, and K_{44}^{L} for a LO phonon. The values of p, q, and r are equal to the values of p', q', and r', respectively, in diamond-type (homopolar) crystals, but they are different for zinc-blende–type (polar) crystals. In fact their difference can be related to the change of the TO phonon effective charge e^* due to the strains.

The PDP introduced above are linked to the experimental data through the slopes $(d\Omega/dX)$ of the stress-dependent phonon frequencies $\Omega_T(X)$ or $\Omega_L(X)$. The stress is compressive and therefore regarded as negative. Depending on the polarization of the incident light the components of the TO, LO phonons are characterized as singlets (s, for $\mathbf{E}||\mathbf{X}$) or doublets (d, for $\mathbf{E}\perp\mathbf{X}$). This is, because for the crystal orientations b and c used here, the triply degenerate $q\approx 0$ optical phonon is split into a singlet and a doublet (see Fig. 1). If the singlet or either component of the doublet happens to be of longitudinal character then the corresponding frequency is increased by the TO-LO splitting.[1-3] The latter splitting is a function of the stress, in general. Table I summarizes all relevant information such as selection rules, measured slopes and the corresponding PDP that can be calculated from each configuration. The complete expressions are as follows: From configurations b,c ($\mathbf{X}||[001],\mathbf{X}||[111]$)

$$\gamma_T=-\frac{p+2q}{6\omega_T^2}=-\frac{d(\Omega_{T,s}+2\Omega_{T,d})}{dX}\frac{1}{3\omega_T(S_{11}+2S_{12})}\,, \tag{4}$$

$$\gamma_L=-\frac{p'+2q'}{6\omega_L^2}=-\frac{d(\Omega_{L,s}+2\Omega_{L,d})}{dX}\frac{1}{3\omega_L(S_{11}+2S_{12})}\,. \tag{5}$$

From configuration c ($\mathbf{X}||[111]$)

$$\frac{r}{2\omega_T^2}=\frac{d(\Omega_{T,s}-\Omega_{T,d})}{dX}\frac{1}{\omega_T S_{44}}\,, \tag{6}$$

$$\frac{r'}{2\omega_L^2}=\frac{d(\Omega_{L,s}-\Omega_{L,d})}{dX}\frac{1}{\omega_L S_{44}}\,. \tag{7}$$

From configuration b ($\mathbf{X}||[001]$)

$$\frac{p-q}{2\omega_T^2}=\frac{d(\Omega_{T,s}-\Omega_{T,d})}{dX}\frac{1}{\omega_T(S_{11}-S_{12})}\,, \tag{8}$$

$$\frac{p'-q'}{2\omega_L^2}=\frac{d(\Omega_{L,s}-\Omega_{L,d})}{dX}\frac{1}{\omega_L(S_{11}-S_{12})}\,. \tag{9}$$

Crystal orientation a is defined as

$$(x,y,z)=([100],[010],[001])$$

and is equivalent to the configuration b, used here, as far as Table I is concerned. It is included here for completeness (see Table II). In Equations (4)–(9), S_{ij} are the elastic compliances. The values used here are the same as those in Ref. 3, i.e., $S_{11}-S_{12}=1.54$, $S_{11}+2S_{12}=0.445$, and $S_{44}=1.69$ in 10^{-3} kbar^{-1} units. The zero-stress values $\omega_T=268.3$ cm^{-1} and $\omega_L=291.8$ cm^{-1} for the $q\approx 0$, TO and LO phonon frequencies are taken from Ref. 11. The corresponding mode Grüneisen parameters are designated by γ_T and γ_L, respectively. The slopes $(d\Omega/dX)$ were deduced from the spectra in the b,c configurations taken from samples with $N=5\times10^{15}$ and 3.5×10^{17} cm^{-3} and are listed in Table I. A presentation of the data points, consistent with the entries of Table I, is shown in Figs. 3 and 4 for $N=5\times10^{15}$ and 3.5×10^{17} cm^{-3}, respectively. The straight lines are the results of least square calculations. Each pair of points $(\Omega_{T,s},\Omega_{L,s})$ or $(\Omega_{T,d},\Omega_{L,d})$ in Figs. 3 and 4 results from the fitting of a damped harmonic oscillator model to the actual reflectance spectra in the way described in the previous section. The reflectivity R in terms of real (n) and imaginary (k) parts of the complex refractive index is given by

$$R=\frac{(n-1)^2+k^2}{(n+1)^2+k^2}\,, \tag{10}$$

where n,k are obtained from the real and imaginary part

TABLE I. Selection rules, measured slopes (Fig. 3), and phonon deformation potentials (PDP). The arrows indicate which slopes enter the equations for PDP. The slopes and their typical errors are in units of cm^{-1}/kbar. The notation p,q,r and p',q',r' (Refs. 2 and 3) is equivalent to $K_{11}^{T},K_{12}^{T},K_{44}^{T}$ and $K_{11}^{L},K_{12}^{L},K_{44}^{L}$, respectively. For the sign of the slopes we have taken into account that the stress is compressive, therefore negative. The sample orientations used were ($[\bar{1}10],[\bar{1}\bar{1}2],[111]$) and ($[110],[\bar{1}10],[001]$) for $\mathbf{X}||[111]$ and $\mathbf{X}||[001]$, respectively (see Sec. II). The values used for $d\epsilon_\infty/dX$ in Eq. (11) were 0.015 and 0.000 kbar^{-1} for the singlet and doublet components, respectively, for $\mathbf{X}||[111]$. The corresponding values for $\mathbf{X}||[001]$ are 0.014 and 0.001 kbar^{-1}, respectively (see Sec. III A).

Stress direction	Light polarization	Phonon component	Measured slopes $(d\Omega/dX)$ $N=5\times10^{15}$ cm^{-3}	$N=3.5\times10^{17}$ cm^{-3}	Equation	Phonon deformation potentials
$\mathbf{X}||[111]$	$\mathbf{E}||\mathbf{X}$	$\Omega_{T,s}$	-0.249 ± 0.013	-0.176 ± 0.002	→ (6)	$r=K_{44}^{T}$
	$\mathbf{E}\perp\mathbf{X}$	$\Omega_{T,d}$	-0.081 ± 0.009	-0.050 ± 0.003	→ (4)	γ_T
	$\mathbf{E}||\mathbf{X}$	$\Omega_{L,s}$	-0.193 ± 0.012	-0.179 ± 0.004	→ (7)	$r'=K_{44}^{L}$
	$\mathbf{E}\perp\mathbf{X}$	$\Omega_{L,d}$	-0.077 ± 0.007	-0.084 ± 0.003	→ (5)	γ_L
$\mathbf{X}||[001]$	$\mathbf{E}||\mathbf{X}$	$\Omega_{T,s}$	-0.092 ± 0.013	-0.091 ± 0.006	→ (8)	$p-q=K_{11}^{T}-K_{12}^{T}$
	$\mathbf{E}\perp\mathbf{X}$	$\Omega_{T,d}$	-0.123 ± 0.009	-0.156 ± 0.006	→ (4)	γ_T
	$\mathbf{E}||\mathbf{X}$	$\Omega_{L,s}$	-0.019 ± 0.007	-0.005 ± 0.006	→ (9)	$p'-q'=K_{11}^{L}-K_{12}^{L}$
	$\mathbf{E}\perp\mathbf{X}$	$\Omega_{L,d}$	-0.132 ± 0.020	-0.164 ± 0.005	→ (5)	γ_L

TABLE II. Values of the phonon deformation expressions given by Eqs. (4)–(9) for the undoped sample in Table I. Average values of $\gamma_{T,L}$ are computed from corresponding values of configurations b and c. Configuration a corresponds to $(x,y,z)=([100],[010],[001])$.

Crystal orientation	γ_T	γ_L	$\frac{r}{2\omega_T^2}$	$\frac{r'}{2\omega_L^2}$	$\frac{p-q}{2\omega_T^2}$	$\frac{p'-q'}{2\omega_L^2}$	Reference
c	1.15±0.06	0.89±0.05	−0.37±0.03	−0.24±0.03			Present
	0.92±0.10	0.80±0.10	−0.40±0.06	−0.27±0.06			Ref. 4
	1.00±0.30	1.00±0.15	−0.40±0.20	−0.30±0.08			Ref. 2
			−0.10±0.10				Ref. 3
b	0.94±0.06	0.73±0.10			0.08±0.03	0.25±0.05	Present
	0.78±0.10	0.66±0.10			0.12±0.07		Ref. 4
	0.70±0.30	0.80±0.15			0.30±0.15	0.35±0.08	Ref. 2
					0.10±0.10		Ref. 3
a						0.23±0.06	Ref. 4
average	1.05±0.11	0.81±0.10					Present
	0.85±0.10	0.73±0.10					Ref. 4
	0.85±0.30	0.90±0.15					Ref. 2
	0.90±0.30						Ref. 3
hydrostatic	1.39±0.02	1.23±0.02					Ref. 11

of the dielectric constant, $\epsilon=\epsilon_1+i\epsilon_2=(n^2-k^2)+i(2nk)$. The dielectric function used is

$$\epsilon(\omega)=\epsilon_\infty\left[1+\frac{\omega_L^2-\omega_T^2}{\omega_T^2-\omega^2-i\omega\Gamma_T}-\frac{\omega_p^2}{\epsilon_\infty(\omega^2+i\omega\Gamma_e)}\right], \quad (11)$$

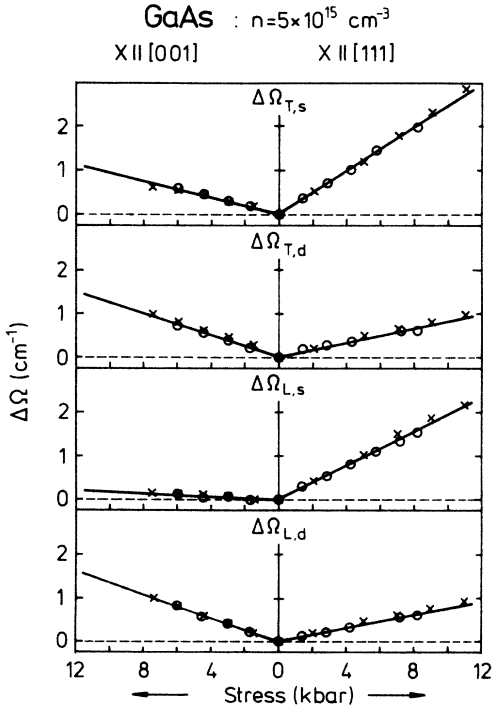

FIG. 3. Stress dependence of phonon frequency shifts $\Delta\Omega$ for undoped GaAs ($N=5\times10^{15}$ cm^{-3}). The uncertainties of the shifts are within 0.025 cm^{-1}. Straight lines are least-square fits for the joint data of two identical samples (× and ○). Their slopes are tabulated in Table I. The zero-stress values of ω_T and ω_L are 268.3 and 290.8 cm^{-1}, respectively.

where $\epsilon_\infty=10.9$ (Ref. 7), the high-frequency value of $\epsilon(\omega)$, Γ_T and Γ_e the damping constant for the TO phonon and for the free carriers, and ω_p the plasma frequency for the free carriers, given by

$$\omega_p=\left[\frac{Ne^2}{\epsilon_0 m^*}\right]^{1/2}. \quad (12)$$

N is the carrier concentration and m^* the corresponding

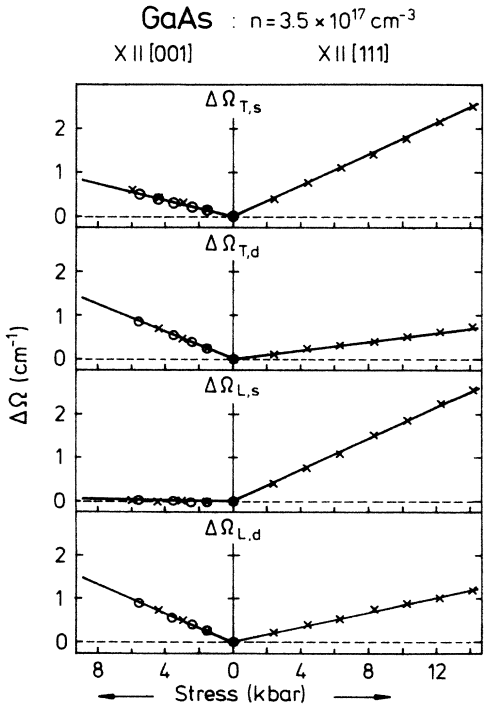

FIG. 4. The same as Fig. 3 but for a doped GaAs sample ($N=3.5\times10^{17}$ cm^{-3}).

effective mass. At this point it should be recognized that the phonon shifts with stress are, in general, different for pure and doped samples, thus leading to different values for PDP. Since one of the objectives of this work is to reach accurate values of PDP for the pure lattice, we shall concentrate on the results of PDP obtained from pure materials. For completeness we also give values of PDP obtained from doped samples. Measurements with doped samples, however, are necessary in order to investigate the stress dependence of the plasma edge. The observed dependence of PDP on carrier concentration is an interesting experimental fact which deserves an independent study.

Regardless of concentration, the fitting procedure was the same and can be described as follows: Fitting with equations (10)—(12) was performed to single spectra $R(\omega,X)$ as well as to the ratios $R(\omega,X)/R(\omega,X=0)$. The latter are very sensitive to small changes, while the former allows a judgement on the quality of the harmonic oscillator approximation through direct comparison of theory and experiment. The fitting procedure was started with the ratios, in order to find out if the sensitivity of the equipment (detector, light source) had changed between scans. Such a change causes a parallel vertical shift of the ratioed spectra [see Fig. 2(b)] and can be taken into account afterwards by multiplying with a factor f giving the corrected spectrum $R'(\omega,X)$:

$$R'(\omega,X)=fR(\omega,X) . \tag{13}$$

Next we tried to improve the fit parameters by achieving best agreement with $R'(\omega,X)$ [Fig. 2(a)]. The quality of the fits was judged from agreement with the measured spectra especially at the edges of the reststrahlen band and the plasma edge, which are important for the phonon and plasma frequencies. With those parameters the ratioed spectra were fitted again, this time giving a better value for f. This iterative procedure was repeated until agreement between harmonic oscillator and measurement was within 0.025 cm^{-1} for phonon frequencies and 0.25 cm^{-1} for the plasma frequency ω_P in doped samples. The absolute accuracy is less for the plasma frequency because the reflectivity slope is smaller than the one in the phonon reststrahlen band. However, since the stress-induced shifts for the plasma edge were larger than for the reststrahlen band, the same relative accuracy was obtained for the stress-induced changes of ω_P. A typical fit is shown in Fig. 2(b).

Inspection of Fig. 2 and Eqs. (10)—(12) tells us that besides ω_T and ω_L, the stress X will also induce changes in the values of ϵ_∞, Γ_T, Γ_e, and m^*. Thus, through careful fitting one should be able, in principle at least, to obtain information about the corresponding slopes. In the case of ϵ_∞ and N we have calculated the slopes by use of the compliance coefficients[3] and the photoelastic constants.[12,13] In all previous calculations[4,7] the photoelastic constants of Ref. 13 measured at 1.15 μm were used. Here we prefer to use values which were obtained from the data of Ref. 12. These data show that there is still dispersion in the photoelastic constants in the near infrared region originating from the electronic band gaps. By extrapolating these results [Eqs. (3)—(9) in Ref. 12] to the far infrared region we obtain nearly constant values and slopes, which are quoted in Tables I and III, respectively. These values were used in the fitting procedure with Eq. (11). In order to facilitate the fitting we incorporate the anticipated values of $\epsilon_\infty(X)$ and $N(X)$ in Eq. (11) and focus on K_{ij}^T, K_{ij}^L, $\Gamma_T(X)$, $\Gamma_e(X)$ (see Sec. IV) and $m^*(X)$ (see Sec. V).

B. Numerical results on PDP

The results of the calculations of the PDP expressions in Eqs. (4)—(9) based on the slopes in Table I, are shown in Table II. The results of other workers are also included in Table II for comparison. The errors indicated originate from the average errors in the slopes from two different samples (Table I) and represent mean-square deviations. Individual values for p,q are obtained from the values of $p-q$ and average γ_T [or $p+2q$, according to Eq. (4)], and likewise for p',q'. These are shown in Table III in suppressed tensor notation. Various microscopic fourth-rank tensor parameters are also included in Table III. The corresponding errors are related to those described above. All values (and their errors) in Table III have been rounded to one decimal point. For more details about these parameters the reader is referred to Ref. 7. For completeness we give the basic definitions below:

$$K_{ij}^{T,L}=(\partial\Omega_{T,L}^2/\partial\eta)_{ij} , \tag{14}$$

$$M_{ij}=(\partial e^*/\partial\eta)_{ij} \tag{15a}$$

$$=\frac{e^*}{2}\left[\frac{\epsilon_\infty}{\omega_T^2\Delta\epsilon}(K_{ij}^L-K_{ij}^T)+\frac{k_{ij}^e}{\epsilon_\infty}+1\right], \quad i,j=1,2,3 \tag{15b}$$

$$=\frac{e^*}{2}\left[\frac{\epsilon_\infty}{\omega_T^2\Delta\epsilon}(K_{ij}^L-K_{ij}^T)+\frac{k_{ij}^e}{\epsilon_\infty}\right], \quad i,j=4,5,6 , \tag{15c}$$

$$a_{ij}=\left[\frac{2M_{ij}}{e^*}-1\right]\omega_T^2\Delta\epsilon, \quad i,j=1,2,3 \tag{16a}$$

$$=\frac{2\omega_T^2\Delta\epsilon M_{ij}}{e^*}, \quad i,j=4,5,6 , \tag{16b}$$

$$b_{ij}=-\omega_T^2\Delta\epsilon K_{ij}^T , \tag{17}$$

$$k_{ij}^0=(\partial\epsilon_s/\partial\eta)_{ij} \tag{18a}$$

$$=\epsilon_s(K_{ij}^L/\omega_L^2-K_{ij}^T/\omega_T^2+k_{ij}^e/\epsilon_\infty) \tag{18b}$$

$$=k_{ij}^e+a_{ij}/\omega_T^2+b_{ij}/\omega_T^4 , \tag{18c}$$

$$a_{11}-a_{12}=\epsilon_\infty[(K_{11}^L-K_{12}^L)-(K_{11}^T-K_{12}^T)]+\frac{\omega_T^2\Delta\epsilon}{\epsilon_\infty}(k_{11}^e-k_{12}^e) , \tag{19}$$

$$\frac{M_{11}-M_{12}}{e^*}=\frac{(a_{11}-a_{12})}{2\Delta\epsilon\omega_T^2} , \tag{20}$$

$$k_{ij}(\omega)=k_{ij}^e+\frac{a_{ij}}{(\omega_T^2-\omega^2)}+\frac{b_{ij}}{(\omega_T^2-\omega^2)^2} , \tag{21}$$

$$\gamma^* = -\left[\frac{\partial \ln e^*}{\partial \ln V}\right] = -\frac{M_{11}+2M_{12}}{3e^*} \tag{22a}$$

$$= \frac{\epsilon_s}{\Delta\epsilon}\gamma_L - \frac{\epsilon_\infty}{\Delta\epsilon}\gamma_T - \frac{k_{11}^2+2k_{12}^2}{6\epsilon_\infty} - \frac{1}{2} . \tag{22b}$$

V is the crystal volume, ϵ_∞ and ϵ_s are the high- and low-frequency values of the dielectric constant and likewise for the photoelastic constants k_{ij}^e and k_{ij}^0, while $\Delta\epsilon=\epsilon_s-\epsilon_\infty=1.99$ for GaAs. Two sets of calculated values are included in Table III based on the present data. One set is based on the photoelastic constants of Ref. 13 and is included here for comparison with the sets of Refs. 2, 4, and 7 for which the same values k_{ij}^e of Ref. 13 were used. The other set was based on k_{ij}^e values which were obtained by extrapolating from the data of Ref. 12 (see Sec. II A). The differences between the two sets are well within the experimental errors. Finally, it is clear from Eqs. (15), (19), and (20) how the value of the strain-dependent effective charge is affected by the differences between the values of K_{ij}^L and K_{ij}^T, respectively. The tensors a_{ij} and b_{ij} determine, through Eq. (21), the dispersion of $k_{ij}(\omega)$ in the infrared [ionic photoelastic effect, Ref. (7)].

Among the various published sets of results appearing in Table III, only the one under Ref. 4 is based on piezo-Raman data. (No attempt was made to obtain a set of values based on the original piezo-Raman data of Ref. 3

TABLE III. Numerical values for the three components of the various tensor properties, based on the present data for the undoped sample of Table I, and those of other workers. The values of $(k_{11}^e,k_{12}^e,k_{44}^e)$ used here are either (17.5,8.7,8.5) from Ref. 12 or (19.6,16.63,8.55) from Ref. 13. Direct use of Eq. (16a) for $a_{11}-a_{12}$ leads to a more realistic error figure.

	$(i,j)=(1,1)$	$(i,j)=(1,2)$	$(i,j)=(4,4)$	Reference
K_{ij}^T/ω_T^2	−1.8±0.1	−1.9±0.1	−0.7±0.1	Present
	−1.4±0.2	−1.6±0.2	−0.8±0.1	Ref. 4
	−1.3±0.7	−1.9±0.6	−0.8±0.4	Ref. 2
	−2.4±0.2	−3.0±0.1	−0.8±0.4	Ref. 7
K_{ij}^L/ω_L^2	−1.1±0.2	−1.6±0.2	−0.5±0.1	Present
	−1.0±0.2	−1.5±0.2	−0.5±0.1	Ref. 4
	−1.3±0.3	−2.0±0.3	−0.6±0.2	Ref. 2
	−2.0±0.1	−2.7±0.1	−0.6±0.2	Ref. 7
M_{ij}/e^*	2.6±0.6	1.0±0.8	0.9±0.3	Present[a]
	2.7±0.6	1.3±0.8	0.9±0.3	Present
	1.9±0.9	1.0±0.9	0.8±0.5	Ref. 4
	0.7±2.0	−0.1±1.9	0.6±1.2	Ref. 2
	1.5±0.7	0.7±0.4	0.6±1.2	Ref. 7
	1.7	0.1	0.9	Ref. 14
a_{ij}/ω_T^2	8.3±2.4	1.8±3.3	3.6±1.1	Present[a]
	8.7±2.4	3.3±3.3	3.6±1.1	Present
	5.6±3.7	1.9±3.5	3.3±2.0	Ref. 4
	0.6±8.0	−2.4±7.7	2.6±4.8	Ref. 2
	3.9±2.6	0.8±1.5	2.6±4.8	Ref. 7
	4.6	−1.6	3.5	Ref. 14
b_{ij}/ω_T^4	3.6±0.2	3.9±0.2	1.5±0.1	Present
	2.8±0.4	3.2±0.4	1.6±0.2	Ref. 4
	2.6±1.4	3.8±1.2	1.6±0.8	Ref. 2
	4.8±0.4	6.0±0.2	1.6±0.8	Ref. 7
k_{ij}^0	29.4±2.6	14.4±3.4	13.6±1.2	Present[a]
	31.8±2.6	23.8±3.4	13.6±1.2	Present
	28.0±3.7	21.8±3.5	13.4±2.0	Ref. 4
	28.2±2.7	23.4±1.5	12.7±3.9	Ref. 7
	$(a_{11}-a_{12})/\omega_T^2$	$(M_{11}-M_{12})/e^*$	γ^*	Reference
	6.5±1.4	1.6±0.4	−1.5±0.9	Present[a]
	5.4±1.4	1.4±0.4	−1.8±0.9	Present
	3.7±2.2	0.9±0.6	−1.3±0.7	Ref. 4
	3.0±3.0	0.8±0.8	−1.0±0.3	Ref. 7
			−0.7	Ref. 11
	6.2	1.6	−0.6	Ref. 14

[a]Based on $(k_{11}^e,k_{12}^e,k_{44}^e)$ from Ref. 12. In all other cases the values of Ref. 13 have been used.

because the latter are incomplete and suffer from large uncertainties.) The remaining three sets are based on reflectance data. In all sets (except the one under Ref. 7) the corresponding average experimental values $\gamma_{T,L}$ are used in the calculation. In Ref. 7 the values of $\gamma_{T,L}$ from hydrostatic pressure measurements were used.[11] The set of values under Ref. 14 represents the results of a calculation based on a semiempirical bond-orbital model for the effective charge.

Ignoring for the moment the errors in the entries of Table III, and judging at least from the present results and those under Refs. 4 and 14 we can say that the various values agree to within less than a factor of 2. In the case of a_{12} the apparent disagreement becomes meaningless if the corresponding uncertainties are taken into consideration. As previously suggested[2,3,7] the systematically lower values for the Grüneisen coefficients found in all uniaxial stress experiments, compared to the values from hydrostatic pressure work,[11] are attributed to stress relaxations on the sample surface and along the penetration depth of the probing radiation. As suggested in Ref. 15, such relaxations may also depend on the direction of incidence, that is, the choice of reflecting or scattering crystal plane.

IV. UNIAXIAL STRESS AND PHONON DAMPING CONSTANTS

The damping constants of the TO and LO phonons are, in general, expected to be influenced by an external uniaxial stress or a hydrostatic pressure, through the effects that such generalized forces have on the lattice anharmonicity. At present we are not aware of any phenomenological or microscopic theoretical treatment of the problem. In principle such changes should be detected in reflectance experiment, whereby slopes of the form $(\partial\Gamma_T/\partial\eta)$ could be inferred from data analogous to those of $\Omega_{T,s}$ and $\Omega_{T,d}$ (Fig. 3). It is noted, however, that only Γ_T can be studied in this way and not Γ_L, since the latter does not enter in Eq. (11). Information about Γ_L can be obtained from piezo-Raman experiments by use of appropriate selection rules.

Besides obtaining a value of $\Gamma_T=2.3$ cm^{-1} from the fitting, reliable results for $(\partial\Gamma_T/\partial\eta)$ were not possible in the present measurements because of experimental and computational limitations. The following representative values were obtained from the present fitting procedure for $(d\Gamma_T/dX)$: 0.030 ± 0.015 and 0.01 ± 0.01 cm^{-1}/kbar for the singlet and doublet components, respectively, with $\mathbf{X}\|[111]$. The values obtained with $\mathbf{X}\|[001]$ were zero within the present accuracy limits. This yields the values -18 cm^{-1} and -6 cm^{-1} for the parameter $(\partial\Gamma_T/\partial\eta)$ for the singlet and doublet phonon components, respectively, when $\mathbf{X}\|[111]$. The minus sign is due to the compressive character of $\mathbf{X}$. These are much smaller than the absolute value of 300 cm^{-1} which was used in Ref. 7. [The latter value was based on an upper limit for the apparent broadening at the average rate of 3 cm^{-1}/kbar (Evans and Ushioda, Ref. 6), and on an erroneous[16] average compliance coefficient $\bar{S}=10^{-2}$ kbar^{-1}. Here we use the value $S_{44}=1.69\times10^{-3}$ kbar which is appropriate for the present geometry.]

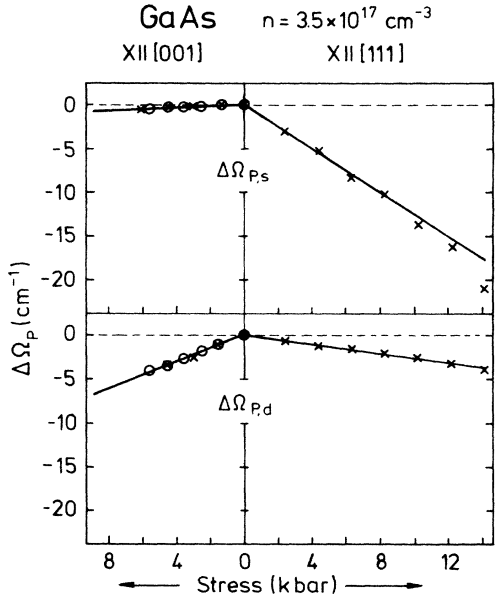

FIG. 5. Stress dependence of plasma frequency shifts $\Delta\Omega_P$ for doped GaAs ($N=3.5\times10^{17}$ cm^{-3}). The uncertainties of the shifts are within 0.25 cm^{-1}. The zero stress value of ω_P is 660 cm^{-1}. The corresponding slopes are tabulated in Table IV.

V. STRESS DEPENDENCE OF PLASMA FREQUENCIES

The stress dependence of the plasma frequency [Eq. (12)] as obtained from the fitting procedure is displayed in Fig. 5. With one exception, we observe a strong decrease of Ω_P with increasing stress. As will be shown in the following analysis, such a decrease is mainly caused by the increase of the effective mass. A phenomenological formulation of the effect of a uniaxial stress on the plasma frequency ω_P can be approached in the same way as for the $q\approx0$ optical phonons. In the absence of any stress the plasma frequency for zinc-blende structures is isotropic (degeneracy 3). The degeneracy is reduced in the presence of a uniaxial stress, due to changes in the effective mass. For the present directions of stresses, ω_P splits into a singlet ($\Omega_{P,s}$ for $\mathbf{E}\|\mathbf{X}$) and a doublet ($\Omega_{P,d}$ for $\mathbf{E}\perp\mathbf{X}$). The corresponding plasmon deformation potentials (PLDP) $K^{FC}_{\lambda\mu\rho\sigma}$ are defined in the same way as the phonon deformation potentials of Eq. (14),

$$K^{FC}_{\lambda\mu\rho\sigma}=\left[\frac{\partial\Omega_P^2}{\partial\eta}\right]_{\lambda\mu\rho\sigma}. \tag{23}$$

Using Eq. (12), and after differentiation, we obtain

$$K^{FC}_{\lambda\mu\rho\sigma}=-\omega_P^2\left[\delta_{\lambda\mu}\delta_{\rho\sigma}+\frac{L_{\lambda\mu\rho\sigma}}{m^*}\right], \tag{24}$$

where

$$L_{\lambda\mu\rho\sigma}=\left[\frac{\partial m^*}{\partial\eta}\right]_{\lambda\mu\rho\sigma}. \tag{25}$$

TABLE IV. Changes of plasma frequencies and effective masses with uniaxial stress obtained from fitting the reflectivity spectra of Te-doped GaAs ($N=3.5\times10^{17}$ cm^{-3}) with Eqs. (10)–(12). The zero-stress value of ω_P was 660 cm^{-1}.

Stress direction	Light polarization	Plasma frequency component	Measured slopes $d\Omega_P/dX$ (cm^{-1}/kbar)	Effective masses $\frac{\Delta m^*\times100}{m^*X}$ (kbar^{-1}) Experimental: Present work	Experimental: Cyclotron resonance (Ref. 16)	Theoretical: $\mathbf{k}\cdot\mathbf{p}$ (Ref. 8)
X||[111]	E||X	$\Omega_{P,s}$	1.26±0.05	−0.423±0.015		−0.318
	E⊥X	$\Omega_{P,d}$	0.25±0.05	−0.118±0.015	−0.075±0.015	−0.241
X||[001]	E||X	$\Omega_{P,s}$	0.09±0.01	−0.070±0.004		0.076
	E⊥X	$\Omega_{P,d}$	0.79±0.04	−0.281±0.011	−0.23 ±0.06	−0.469

The three nonvanishing components of $K^{FC}_{\lambda\mu\rho\sigma}$ are related to the measured frequency shifts of $\Omega_{P,s}$ and $\Omega_{P,d}$ through expressions analogous to Eqs. (4)–(9): X||[111] (configuration c, see Sec. III) is

$$\Omega_{P,s}-\Omega_{P,d}=\frac{X}{2\omega_P}S_{44}K^{FC}_{44}\ , \tag{26}$$

$$\Omega_{P,s}+2\Omega_{P,d}=\frac{X}{2\omega_P}(S_{11}+2S_{12})(K^{FC}_{11}+2K^{FC}_{12})\ , \tag{27}$$

X||[001] (configuration b) is

$$\Omega_{P,s}-\Omega_{P,d}=\frac{X}{2\omega_P}(S_{11}-S_{12})(K^{FC}_{11}-K^{FC}_{12})\ , \tag{28}$$

$$\Omega_{P,s}+2\Omega_{P,d}=\frac{X}{2\omega_P}(S_{11}+2S_{12})(K^{FC}_{11}+2K^{FC}_{12})\ . \tag{29}$$

The components of $L_{\lambda\mu\rho\sigma}$ in suppressed index notation are then obtained from (24) as

$$L_{ij}=-m^*\left[1+\frac{K^{FC}_{ij}}{\omega_P^2}\right],\quad i,j=1,2,3\ , \tag{30}$$

$$L_{ij}=-m^*\frac{K^{FC}_{ij}}{\omega_P^2},\quad i,j=4,5,6\ . \tag{31}$$

Furthermore, the counterpart of the Grüneisen parameter for the plasma frequency ω_P is conveniently defined as

$$\gamma^{FC}=-\frac{\partial\ln\Omega_P}{\partial\ln V}=-\frac{K^{FC}_{11}+2K^{FC}_{12}}{6\omega_P^2}=-\frac{d(\Omega_{P,s}+2\Omega_{P,d})/dX}{3\omega_P(S_{11}+2S_{12})} \tag{32}$$

following Eq. (4). The measured slopes for the various components are listed in Table IV, while in Table V the results of the calculations are included, concerning the PLDP, the effective mass deformation potentials L_{ij}, and the plasmon Grüneisen parameter γ^{FC}.

In terms of the effective mass deformation potentials L_{ij}, the singlet (m_s^*) and doublet (m_d^*) components of m^* can be written, after some straightforward calculations, as

$$m_s^*=m^*+(S_{11}L_{11}+2S_{12}L_{12})X\ , \tag{33}$$

$$m_d^*=m^*+[S_{12}L_{11}+(S_{11}+S_{12})L_{12}]X\ . \tag{34}$$

With these equations one can obtain the slopes of $\Delta m^*/m^*$ versus stress X from the data in Fig. 5. These values are also listed in Table IV. Values for E⊥X have been obtained from cyclotron resonance measurements.[17] They compare well for X||[001] but not for X||[111]. For the direction E||X (i.e., effective mass along the stress direction) no experimental values seem to be published in the literature. However, theoretical values, involving $\mathbf{k}\times\mathbf{p}$ calculations, have been quoted for GaAs in both stress directions[8] (see Table IV). Their tendency describes very well the experiment, but quantitative agreement probably has to await more accurate values for the deformation potentials of the higher electronic conduction bands used in these calculations.

VI. CLOSING REMARKS

From the present investigation it has become clear that relatively reliable values can be reached for PDP from IR (infrared) reflectivity measurements in good agreement

TABLE V. Deformation potentials of plasma frequencies and effective masses as defined in Eqs. (23), (25), and (32) rounded to two decimal points.

	$(i,j)=(1,1)$	$(i,j)=(1,2)$	$(i,j)=(4,4)$
K^{FC}_{ij}/ω_P^2	2.83±0.12	4.20±0.19	1.81±0.13
L_{ij}/m^*	−0.26±0.01	−0.35±0.01	−0.12±0.01
γ^{FC}	1.92±0.09		
	3.12[a]		

[a]From hydrostatic pressure experiments, Ref. 20.

with the results of piezo-Raman spectroscopy. It appears that with the conventional far-infrared or Raman spectroscopic techniques, the limit of accuracy is reached. For more accurate measurements of phonon shifts and damping constant changes, one should think in terms of a different experimental approach. Table I implies that the PDP values are affected by the carrier concentration. The conclusions of other workers (Ref. 2 for GaAs, Refs. 18 and 19 for Si and GaP, respectively) do not contradict this observation. In this connection it should be noted that Eqs. (15)—(22) were derived from a dielectric function similar to that of Eq. (11) but without the plasma term.

It should be interesting, however, to examine theoretically the effect of carrier concentration on the dispersion of photoelastic coefficients, that is, an equation analogous to Eq. (21) completed with plasma terms. Concerning the present observation of $\Omega_P(X)$ we have presented here for the first time a complete set of plasmon deformation potentials, which allow one to determine the anisotropic effective mass tensor in strained GaAs. Uniaxial stress measurements on other III-V materials by use of reflectance and Raman techniques are now in progress.

ACKNOWLEDGMENTS

This work was supported by the Stiftung Volkswagenwerk (Hannover, Germany). We also acknowledge partial support by the Greek and German Ministries on Research and Technology.

[1]E. Anastassakis, in *Dynamical Properties of Solids,* edited by G. K. Horton and A. A. Maradudin (North-Holland, Amsterdam, 1980), Vol. 4, p. 157.

[2]B. A. Weinstein and M. Cardona, Phys. Rev. B **5**, 3120 (1972).

[3]F. Cerdeira, C. J. Buchenauer, F. H. Pollak, and M. Cardona, Phys. Rev. B **5**, 580 (1972).

[4]A. K. Sood, E. Anastassakis, and M. Cardona, Phys. Status Solidi B **129**, 501 (1985). The configurations *b,c* in Ref. 4 differ from the present ones by a 90° rotation about z',z'', respectively, without any consequences as far as the present experiment is concerned.

[5]K. Yamazaki, M. Yamada, K. Yamamoto, and K. Abe, Jpn. J. Appl. Phys. **23**, 681 (1984), and references therein; P. Zorabedian and F. Adar, Appl. Phys. Lett. **43**, 177 (1983); F. Moser and R. Beserman, J. Appl. Phys. **54**, 1033 (1983); H. Tan, M. Knok, S. Ng, C. Ong, and S. Tang, *ibid.* **55**, 1116 (1984).

[6]D. J. Evans and S. Ushioda, Phys. Rev. B **9**, 1638 (1974); E. Liarokapis and E. Anastassakis, *ibid.* **30**, 2270 (1984); H. Shen and F. H. Pollak, Appl. Phys. Lett. **45**, 692 (1984); D. R. Myers, P. L. Gourley, and P. S. Peercy, J. Appl. Phys. **54**, 5032 (1983).

[7]E. Anastassakis, J. Phys. C **16**, 3329 (1983).

[8]D. E. Aspnes and M. Cardona, Phys. Rev. B **17**, 741 (1978).

[9]R. Siedling, J. Saalmüller, and W. Richter (unpublished).

[10]H. Vogelman and T. A. Fjeldly, Rev. Sci. Instrum. **45**, 309 (1974).

[11]R. Trommer, H. Müller, M. Cardona, and P. Vogl, Phys. Rev. B **21**, 4869 (1980).

[12]N. Suzuki and K. Tada, Jpn. J. Appl. Phys. **23**, 1011 (1984).

[13]R. W. Dixon, J. Appl. Phys. **38**, 5149 (1967).

[14]E. Anastassakis and M. Cardona, Phys. Status Solidi B **129**, 101 (1985).

[15]I. I. Novak, V. V. Baptitzmanskii, and L. V. Zhoga, Opt. Spectrosc. **43**, 145 (1977).

[16]In Table 1 of Ref. 7 the values of the elastic compliances S_{ij} were taken from *AIP Handbook of Physics,* 3rd edition, edited by D. E. Gray (McGraw-Hill, New York, 1972). The reader is cautioned in that the values for GaAs are erroneously listed in the above handbook (ten times larger). Here, we use the values from Ref. 3.

[17]J. C. Portal, R. A. Cooke, R. A. Stradling, A. R. Adams, and C. N. Ahmad, Solid State Commun. **34**, 335 (1980).

[18]M. Chandrasekhar, J. B. Renucci, and M. Cardona, Phys. Rev. B **17**, 1623 (1978).

[19]I. Balslev, Phys. Status Solidi B **61**, 207 (1974).

[20]G. D. Pitt, J. Lees, R. A. Hoult, and A. R. Stradling, J. Phys. C **6**, 3282 (1973).